AIP | Journal of Applied Physics

Surfactant enhanced solid phase epitaxy of Ge/CaF2/Si(111): Synchrotron x-ray characterization of structure and morphology

J. Wollschläger, C. Deiter, C. R. Wang, B. H. Müller, and K. R. Hofmann

Citation: J. Appl. Phys. **110**, 102205 (2011); doi: 10.1063/1.3661174
View online: http://dx.doi.org/10.1063/1.3661174
View Table of Contents: http://jap.aip.org/resource/1/JAPIAU/v110/i10
Published by the American Institute of Physics.

Surfactant enhanced solid phase epitaxy of Ge/CaF_2/Si(111): Synchrotron x-ray characterization of structure and morphology

J. Wollschläger,[1,a)] C. Deiter,[2] C. R. Wang,[3] B. H. Müller,[3] and K. R. Hofmann[3]
[1]*Fachbereich Physik, Universiät Osnabrück, Barbarastrasse 7, Osnabrück D-49069, Germany*
[2]*Deutsches Elektronen Synchrotron (DESY), Notkestr. 85, Hamburg, Germany*
[3]*Institute of Electronic Materials and Devices, Leibniz Universität Hannover, Schneiderberg 32, Hannover D-30167, Germany*

(Received 28 September 2010; accepted 26 March 2011; published online 30 November 2011)

The structure and morphology of CaF_2/Si(111) and Ge/CaF_2/Si(111) layered structures with film thicknesses in the range of very few nanometers has been studied with synchrotron-based radiation. While the CaF_2 film is grown via molecular beam epitaxy, the Ge film is fabricated by surfactant enhanced solid phase epitaxy with Sb as surfactant. The CaF_2 film forms two laterally separated phases of relaxed CaF_2 and pseudomorphic CaF_2, respectively, although the film thickness is very homogeneous. The Ge film is completely relaxed and forms A-oriented parts as well as B-oriented parts, due to twinning. In spite of the large surface roughness of the Ge film, it completely wets CaF_2/Si(111) also after annealing at 600 °C, due to the application of Sb during the annealing process.
 [doi:10.1063/1.3661174]

I. INTRODUCTION

For various applications in the fields of microelectronics and nanoelectronics as well as optoelectronics and photovoltaics, it is advantageous to use lattice-matched epitaxial films of insulating materials. For instance, large efforts are made to develop the germanium-on-insulator (GeOI) technique to integrate new materials on the Si technology platform. This technique offers very good possibilities, e.g., to integrate Ge for high speed applications[1–3] or III-V materials for photovoltaic devices on the reasonable Si platform.[4,5]

Here, the use of CaF_2 as insulating material is advantageous, since CaF_2 has an extremely large bandgap (12.1 eV), its cubic crystal structure (fluorite) is similar to the diamond structure of Si, and, finally, the CaF_2 lattice constant matches almost the lattice constant of Si (lattice mismatch 0.6% at room temperature).[6–8] Furthermore, CaF_2 may serve as a perfect intermediate between Si and Ge (lattice mismatch 4.0% with respect to Si) at higher growth temperatures, since the thermal expansion of CaF_2 is much larger than the thermal expansion of both Si and Ge. However, while ultrathin CaF_2 films grow very well on Si(111) (laminar growth mode), due to the low surface energy of CaF_2(0.45 J/m^2) compared to the surface energy of Si (1.24 J/m^2), it is expected that Ge (surface energy 1.06 J/m^2) does not wet CaF_2(Volmer Weber growth mode, 3D island formation).[7] Therefore, techniques have to be developed to surpass the thermodynamic equilibrium of de-wetting.

Early studies on Ge epitaxy on thin CaF_2 films were motivated by microelectronic applications as improved gate insulators and 3D integration.[6] Thus, in these studies, the films of both materials Ge and CaF_2 were several 100 nm thick. On the one hand, the crystalline quality of the Ge films improved with increasing deposition temperature, while, on the other hand, the surface roughness increased too.[10,11] Furthermore, twinning formation has been observed for Ge films (as well as for Si films). The size of Ge crystallites, however, is much larger than the size of Si crystallites, if deposited at the same temperature. The twinning has been attributed to nucleation of both A-oriented and B-oriented semiconductor islands on the B-oriented CaF_2 films. For the B-orientation, the crystal structure is rotated by 180° about the [111] surface normal. The B-orientation of the CaF_2 film is caused by the formation of dissociated CaF at the interface, which improves the binding between the CaF_2 film and Si(111) substrate.[7] Recently, it has been reported from density functional theory (DFT) calculations that similar effects occur at the Ge(111)/CaF_2(111) interface.[12] B-oriented Ge(111) films are favored if fluorine is removed from the CaF_2(111) surface, while, in contrast to A-oriented Si(111) films, A-oriented Ge(111) films are stabilized by F-double layers at the Ge(111)/CaF_2(111) interface.

The roughness of the Ge film, however, could be decreased if, initially, Ge films of nanometer thickness were pre-deposited at room temperature prior to the second growth stage at higher temperatures (typically 600 °C)[13,14] or if the CaF_2 surface was modified by electron beam exposure to remove F from the surface of the CaF_2 film and to increase the binding at the interface between the Ge film and CaF_2 film.[15] The use of nanometer-thick boron films as interfactant has also been demonstrated to improve the quality of the Ge film.[16]

However, Si-based nanoelectronic applications, e.g., resonant tunneling devices, where CaF_2 films and semiconductor films (e.g., Si, Ge) serve as tunneling barriers and quantum wells, respectively, require much higher demands, since all involved films can only have nanometer thickness and have to be atomically smooth.[17] Recently, it has been shown that the homogeneity of Si films deposited on CaF_2/Si(111) is improved if solid phase epitaxy (SPE) is combined with the use of surfactants (e.g., B, Sb), which are deposited

a)Electronic mail: joachim.wollschlaeger@uos.de.

during the annealing.[19–21] Electronic devices, which were fabricated on the base of this technique, perform much better than devices fabricated with other techniques.[22–24] Furthermore, due to its passivating property, the surfactant As has been applied after removal of fluorine from the CaF_2 interface by electron exposure *prior* to Si deposition.[24] This procedure improves the laminar growth of ultrathin Si films with B orientation for deposition at 500 °C.

Here, we report on surfactant-enhanced solid phase epitaxy (SE-SPE) of ultrathin Ge films on CaF_2/Si(111). We use Sb as surfactant, since it was successfully applied as surfactant for Ge/Si(111), switching the growth mode from Stranski-Krastanov to Frank-van der Merve.[25] Compared to Si, Ge has the advantage of lower surface energy (see above). Therefore, the driving force to form islands on CaF_2 films is smaller, but cannot be ignored. Nevertheless, very little is reported on Ge/CaF_2/Si(111) if the thickness of films of both Ge and CaF_2 are in the range of 1 nm necessary to fabricate nanoelectronic devices, since small Ge islands are formed if Ge is deposited at elevated temperatures.[26,27] Despite these difficulties to form homogeneous Ge films of nanometer thickness on CaF_2/Si(111) tunneling diodes with Ge quantum dots embedded in a CaF_2 film, the tunneling barrier exhibits negative differential conductance.[27]

Although room temperature–deposited Ge films of few atomic layer thickness are crystalline and have homogeneous thickness[28] (compared to room temperature–deposited amorphous Si films), it is advantageous to anneal these films in order to improve the crystalline quality of the Ge films. Annealing above 400 °C, however, leads again to complete de-wetting, due to island formation, as proven by x-ray photoelectron spectroscopy (XPS)[29] and combined studies of spot profile analysis of low-energy electron diffraction (SPA-LEED) and Auger electron spectroscopy (AES).[28] Surprisingly, modifications of the CaF_2 film via electron exposure did not improve the annealing behavior.[29]

In our studies, Ge/CaF_2/Si(111) as well as CaF_2/Si(111) structures were characterized by synchrotron radiation–based x-ray techniques as x-ray reflectivity (XRR), x-ray diffraction (XRD), and gracing incidence x-ray diffraction (GIXRD). These investigations were supported by x-ray photoelectron spectroscopy (XPS) and atomic force microscopy (AFM). Here, we will focus on our detailed synchrotron radiation–based studies.

II. EXPERIMENTAL

Both CaF_2/Si(111) and Ge/CaF_2/Si(111) structures were fabricated via molecular beam epitaxy (MBE) under conditions of ultra high vacuum (UHV) in a VG80 Si MBE system. The base pressure in the UHV chamber was less than 10^{-8}Pa. An e-beam evaporator was used to deposit Ge, while both CaF_2 and Sb were evaporated from graphite crucibles. Four-inch n-type Si(111) wafers were used as substrates.

In a first deposition step, 12 triple layer (TL) CaF_2 (3.8 nm) were deposited on Si(111) at 500 °C. Here, TL denotes a molecular layer of CaF_2, which consists of a Ca layer embedded in two F layers. It has been reported previously that almost perfect CaF_2 films with negligible roughness are produced under these conditions.[9,30] For one sample, furthermore, 8.4 nm Ge was additionally deposited on the CaF_2 film at room temperature, as proven *a posteriori* by XRR. This Ge film thickness is equivalent to 26 bilayer (BL) Ge, where BL denotes the crystallographic Ge(111) layer, which combines two mono-atomic Ge layers. After Ge deposition, the sample was annealed to 600 °C and was exposed to additional flux of Sb when the sample temperature reached 400 °C.

The CaF_2/Si(111) and Ge/CaF_2/Si(111) structures were studied with synchrotron radiation at HASYLAB (DESY). Both x-ray reflectivity (XRR) and specular x-ray diffraction (XRD, $\Theta - 2\Theta$ scans) experiments were performed at the beamline W1, while studies with grazing incidence x-ray diffraction (GIXRD) were performed at the beamline BW2. Double-crystal Si monochromators were used to select a wavelength of 1.24 Å (10 keV photons). Crystal truncation rods (CTR) measured under these conditions were analyzed with the program package ANA-ROD,[31] while XRR experiments were analyzed with the homemade software *iXRR*.[32]

III. RESULTS

A. X-ray reflectivity

Figure 1 compares XRR measurements of the two samples before and after deposition of Ge on CaF_2/Si(111). The CaF_2/Si(111) sample (Fig. 1(a)) shows well-developed intensity oscillations (Kissing fringes), which point to a layer thickness of 3.8 nm (12 TL) of the CaF_2 film, due to the periodicity of the intensity oscillations. The long-lasting intensity oscillations indicate that both the surface and the interface of the CaF_2 film are very smooth. Thus, additionally, the XRR intensity has completely been analyzed using the Parratt algorithm,[33] including the roughness model of Nevot-Croce.[34] This analysis (cf. line in Fig. 1(a)) confirms that the CaF_2 layer is 3.8 nm thick and that both the CaF_2/Si(111) interface roughness and the surface roughness of the CaF_2 film are less than 0.1 nm.

The XRR measurement on the Ge/CaF_2/Si(111) sample (Fig. 1(b)) also shows intensity oscillations. On the one hand, for large vertical scattering vectors $Q_\perp$, the periodicity of the intensity oscillations is similar to the CaF_2/Si(111) sample without Ge. On the other hand, a shorter periodicity

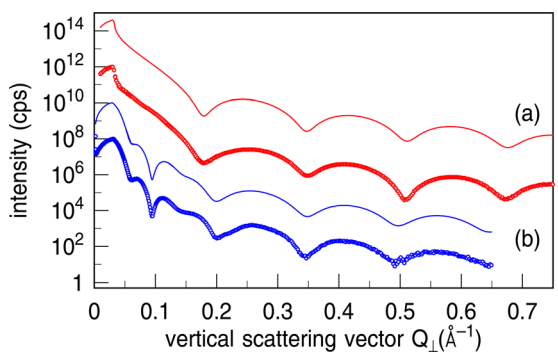

FIG. 1. (Color online) XRR analysis of (a) CaF_2/Si(111) and (b) Ge/CaF_2/Si(111). Dots denote the experimental data, while the solid lines show fitting curves to the data following the Parratt algorithm with modeling of the interface via Nevot-Crocet ansatz.

is observed for smaller scattering angles, due to the increased total film thickness (Ge/CaF_2 double layer). Thus, it can be concluded that the deposited Ge film is very rough compared to the CaF_2 film. The full analysis almost reproduces the characteristics of the CaF_2 film reported above (4.2-nm thickness, roughness of both interfaces less than 0.2 nm). The Ge film, however, is characterized by a film thickness of 8.4 nm (26 BL) and large surface roughness of 4.1 nm. Furthermore, the reduced dispersion of the Ge film points to the formation of islands due to partial de-wetting during the post deposition annealing (PDA).

B. X-ray diffraction

Complementary XRD measurements ($\Theta-2\Theta$ scans) perpendicular to the sample surface and close to the Si(111) Bragg peak are presented in Fig. 2 for both samples CaF_2/Si(111) and Ge/CaF_2/Si(111), respectively. Thus, the scans in reciprocal space are performed in [111] direction. The vertical scattering vector $Q_\perp$ of the XRD scans are scaled to the reciprocal lattice vector of Si by $Q_\perp = \frac{2\pi l}{c_{Si}} (l \in \mathbb{R})$, with $c_{Si} = 313.55$ pm and $\vec{Q} = \frac{2\pi}{c_{Si}}(lll)$.

The diffraction pattern of the CaF_2/Si(111) sample (Fig. 2(a)) exhibits a clear CaF_2(111) Bragg peak very close to the Si(111) Bragg peak. The CaF_2 Bragg peak is broadened, due to the finite CaF_2 film thickness. Compared to the sharp Si(111) Bragg peak, it is slightly shifted to lower l values. The position of the CaF_2 Bragg peak yields a vertical CaF_2 lattice constant of 316 pm, matching the vertical bulk CaF_2(111) lattice constant (315.3 pm) within the experimental error. In addition, well-developed fringes are observed, which confirm the high degree of crystallinity of the CaF_2 film and point to a very homogeneous film thickness. In agreement with the XRR analysis presented above, the periodicity of the intensity oscillations point to a *crystalline* film thickness of 3.9 ($\pm$0.1) nm.

After Ge deposition, clear changes of the XRD diffraction pattern are observed (cf. Figure 2(b)). A Ge(111) Bragg peak emerges at $l = 0.964(\pm 0.003)$, pointing to a vertical Ge lattice constant $c_{Ge} = 325(\pm 1)$ pm (cf. bulk value: 326.638 pm). Thus, the Ge film is almost perfectly relaxed perpendicular to the surface.

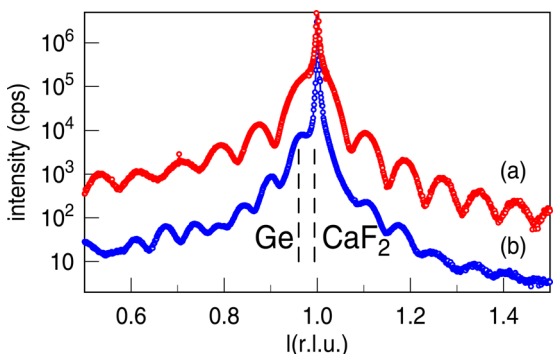

FIG. 2. (Color online) XRD characterization of (a) CaF_2/Si(111) and (b) Ge/CaF_2/Si(111). The (111) Bragg peak of the Si substrate is at $l = 1$. Dashed lines show the positions of bulk Ge and bulk CaF_2, respectively. The well-developed fringes point to very homogeneous films.

On the one hand, the periodicity of the fringes is generally shorter than for the CaF_2/Si(111) sample, due to the increased total film thickness (CaF_2 film and additional Ge film). On the other hand, the periodicity of the fringes is not constant, but depends on the vertical scattering vector. It is shorter for scattering vectors close to the Bragg peaks, while it becomes larger if the scattering vector deviates more from the Bragg condition. This effect can be attributed to the large roughness of the Ge film already observed in the XRR experiments. The roughness of the Ge film decreases the Ge diffraction signal for scattering vectors, which deviate significantly from the Ge Bragg condition, so that interference effects are only well pronounced close to Bragg peaks. Furthermore, the intensity of the fringes shows some beating, pointing to the fact that the CaF_2 film and the Ge film have similar but not identical thickness. It can be estimated from a simple and very rough analysis based on the periodicity of the fringes close to the Bragg peaks and on the beating periodicity that the CaF_2 film thickness and the Ge film thickness are 15 TL and 21 BL, respectively. This result reasonably agrees with the XRR analysis.

Furthermore, Fig. 3 presents in-plane scans in $[1\bar{1}0]$ direction for different vertical scattering vectors $\frac{2\pi}{c_{Si}}(lll)$, which correspond to intensity maxima of the out-of-plane scan shown in Fig. 2(b). Thus, the lateral scattering vector is denoted by $(h\bar{h}0)$. The out-of-plane scans exhibit very sharp peaks at $h = 0$, due to the crystal truncation rod (CTR) of the Si(111) substrate. Additional broad peaks appear at the same position, due to the lateral disorder of the epitaxial films. The broad but intense peak at $l = 0.96$ is caused by the

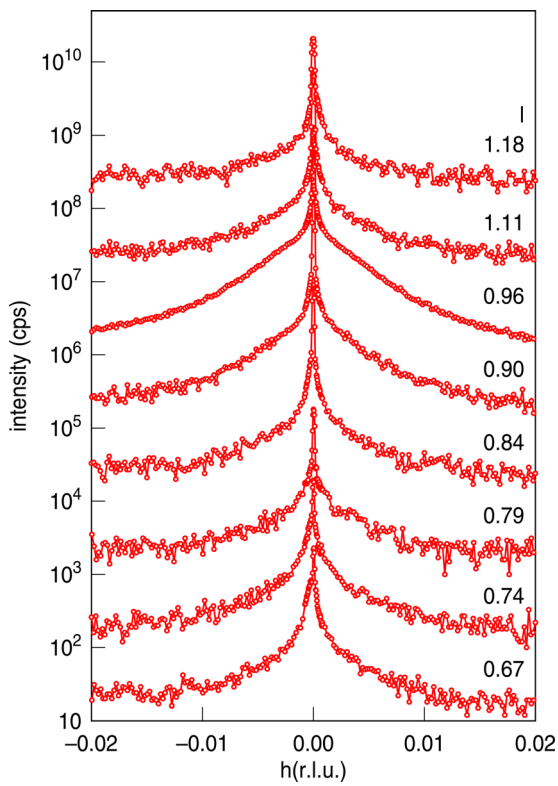

FIG. 3. (Color online) In-plane scans for Ge/CaF_2/Si(111) with fixed vertical scattering vector $\frac{2\pi}{c_{Si}}(lll)$. The broad but intense peak for $l = 0.96$ is caused by the relaxed Ge film.

relaxed Ge film. Fitting this peak with a Lorentzian-like function yields the lateral grain size of 60 nm for the Ge film. Obviously, the broad peak becomes sharper for smaller vertical scattering vectors. Since the Ge film does not contribute to the diffraction signal, due to the large roughness of the Ge film, this peak is governed by the diffraction signal from the CaF_2 film (cf. Figure 2(b)) and can be assigned to a lateral size of 160 nm for the CaF_2 film.

C. Grazing incidence x-ray diffraction

Additional GIXRD experiments have been performed to enhance the sensitivity of the x-ray diffraction investigations to the epitaxial films and to obtain information concerning the lateral order of the film structures. Finite size effects of the ultrathin films as well as the half infinite substrate lead to the formation of crystal truncation rods (CTRs). Therefore, in the following, we will use the surface notation (cf. Fig. 4 and Table I) instead of the bulk notation used before for XRD.

1. CaF_2/Si(111)

First, high resolution in-plane scans were performed on the CaF_2/Si(111) sample to study the degree of lateral relaxation of the CaF_2 film after deposition on Si(111). These experiments are presented in Fig. 5. In-plane (KKL) scans with variable K and fixed L close to $L=0$ (Si Bragg condition on the (11L) CTR) show very sharp peaks, due to the Si(111) substrate and an additional shoulder. The maximum intensity of the shoulder is shifted to lower values of the lateral scattering vector ($H=K<1$). Thus, the shoulder can (at least) partly be attributed to laterally relaxed CaF_2. Superposed to the diffraction signal of the relaxed CaF_2 film, however, disorder at the CaF_2-Si interface as well as pseudomorphic CaF_2 can cause additional diffuse scattering and additional diffraction intensity due to constructive interference, respectively. For detailed analysis, we fitted the in-plane scans to a superposition of three peaks, due to relaxed CaF_2 and pseudomorphic CaF_2 as well as diffuse scattering (due to interface roughness). The result for $L=0.03$ is presented with solid and dashed lines in Fig. 5.

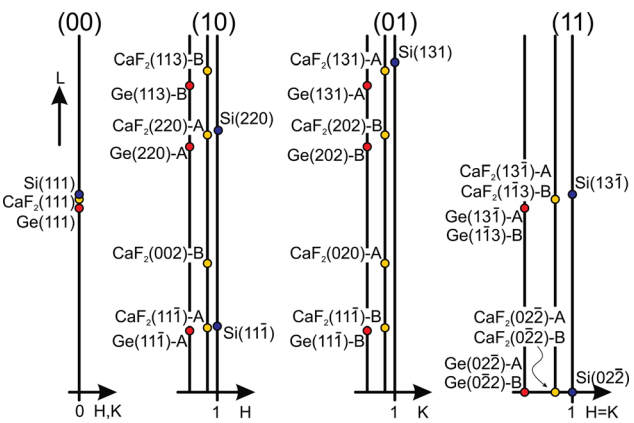

FIG. 4. (Color online) Schematical drawing of the reciprocal space assuming bulk lattice constants of Si, CaF_2, and Ge as well as both A orientation and B orientation of the epitaxial CaF_2 film and Ge film, respectively.

TABLE I. Bulk and surface notation for the Bragg conditions of Si substrate and completely relaxed CaF_2 and Ge films (cf. Fig. 4). The surface indices are scaled with respect to the reciprocal space of the underlying Si substrate.

CTR	Material	Bulk	Surface
(00)	Si	(111)	(0, 0, 1)
	CaF_2		(0, 0, 0.994)
	Ge		(0, 0, 0.960)
(10)	Si	(11$\bar{1}$)	(1, 0, 1/3)
	CaF_2-A		(0.994, 0, 0.331)
	Ge-A		(0.960, 0.320)
	CaF_2-B	(002)	(0.994, 0, 0.663)
	Si	(220)	(1, 0, 4/3)
	CaF_2-A		(0.994, 0, 1.325)
	Ge-A		(0.960, 0, 1.280)
	CaF_2-B		(0.994, 0, 1.657)
	Ge-B		(0.960, 0, 1.600)
(01)	CaF_2-B	(11$\bar{1}$)	(0, 0.994, 0.331)
	Ge-B		(0, 0.960, 0.320)
	CaF_2-A	(020)	(0, 0.994, 0.663)
	CaF_2-B	(202)	(0, 0.994, 1.325)
	Ge-B		(0, 0.960, 1.280)
	Si	(131)	(0, 1, 5/3)
	CaF_2-A		(0, 0.994, 1.657)
	Ge-A		(0, 0.960, 1.600)
(11)	Si	(02$\bar{2}$)	(1, 1, 0)
	CaF_2-A/B	(02$\bar{2}$)/(0$\bar{2}$2)	(0.994, 0.994, 0)
	Ge-A/B	(02$\bar{2}$)/(0$\bar{2}$2)	(0.960, 0.960, 0)
	Si	(13$\bar{1}$)	(1, 1, 1)
	CaF_2-A/B	(13$\bar{1}$)/(1$\bar{1}$3)	(0.994, 0.994, 0.994)
	Ge-A/B	(13$\bar{1}$)/(1$\bar{1}$3)	(0.960, 0.960, 0.960)

Since the superposition of diffraction intensity due to the Si substrate complicates the diffraction analysis for the (11L) CTR, in-plane scans are also recorded on the (01L) CTR close to $L=1/3$, where the CaF_2 film has a Bragg peak due to its B-orientation, while the Si substrate does not have any significant diffraction signal, except some remaining very low intensity of its CTR. This contribution, however, can be neglected, since all Si Bragg conditions are far away (cf. schematic drawing of Fig. 4). These ($0KL$) scans with variable K and fixed L are also shown in Fig. 5. The splitting of the CaF_2 Bragg peak in two components is clearly resolved. The positions of these peaks have been determined by fitting to two Lorentzian-like functions, yielding peak positions at $K=0.994$ and $K=1.000$. Therefore, the peaks can be assigned to relaxed and pseudomorphic CaF_2 phases, respectively, as previously reported for thinner CaF_2 films.[35] The smaller intensity of the peak due to relaxed CaF_2 ($K=0.994$), shows that the majority of the CaF_2 film is pseudomorphic. In agreement with Ref. 35, we conclude from the complete analysis of the L dependence of the in-plane scans ($L=0.10$–0.35) that both phases are laterally arranged and have a thickness of 12 TL. The lateral grain size of the relaxed and pseudomorphic CaF_2 phases is 60 nm and 100 nm, respectively, as concluded from the FWHM of both peaks.

Out-of-plane scans have been performed with lower lateral resolution for the (10L), (01L), and (11L) CTRs. Rotating the sample with respect to the surface normal,

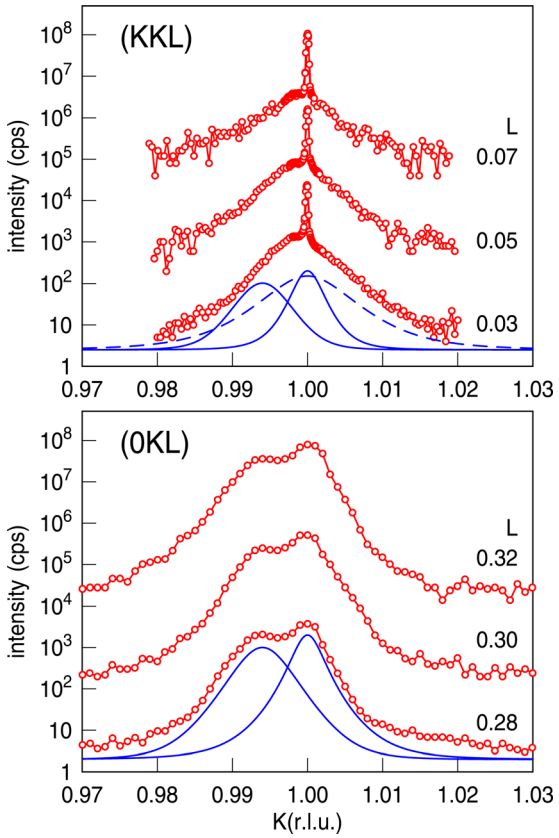

FIG. 5. (Color online) In-plane scans with GIXRD geometry for CaF_2/Si(111): (11L) CTR (top) and (01L) CTR (bottom). The splitting of the CaF_2 Bragg peak into two peaks points to coexisting relaxed and pseudomorphic CaF_2 phases. The solid lines denote Lorentzian-like contributions due to relaxed CaF_2(left) and pseudomorphic CaF_2(right). The dashed line shows additional intensity attributed to diffuse scattering at the rough CaF_2-Si interface. All fitting curves are shifted for clarity.

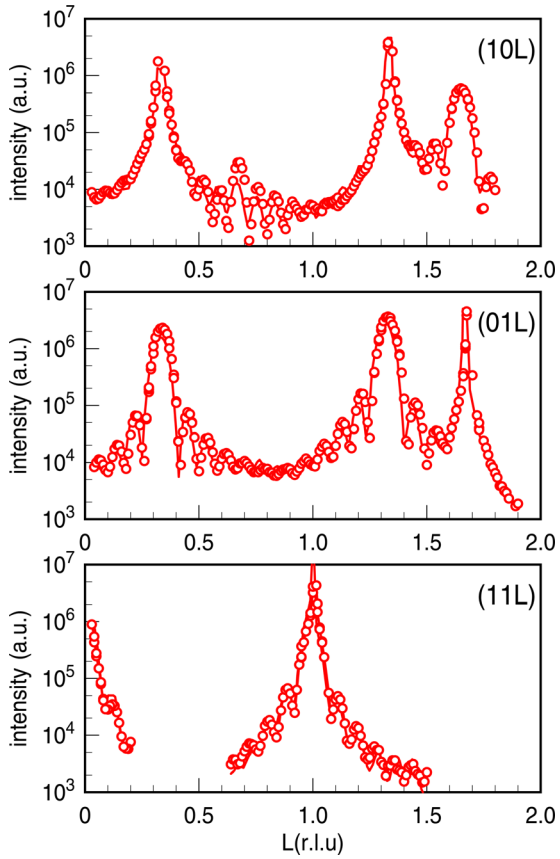

FIG. 6. (Color online) CTR analysis of the (10L) CTR, (01L) CTR, and (11L) CTR (from top to bottom) for CaF_2/Si(111). Open dots are experimental results, while the solid lines show the diffraction analysis following kinematic diffraction theory to obtain structural data. The CaF_2 Bragg peaks show that the CaF_2 is B oriented to an overwhelming extent. The CaF_2 film is very homogeneous, as concluded from well-developed fringes.

complete peaks have been recorded in GIXRD geometry with a fixed value of L to determine the structure factor after subtracting the background intensity from the measured intensity. The integral peak intensities of these CTRs are presented in Fig. 6. Besides the strong Bragg peaks, due to the Si(111) substrate (cf. Figure 4 and Table I), these CTRs show broad CaF_2 Bragg peaks, due to the B-oriented CaF_2 film, as well as fringes, due to the excellent homogeneity of the CaF_2 film thickness (12TL CaF_2, as determined from the periodicity of the fringes). The CaF_2 film is almost entirely B-oriented, as can be judged from the (01L) CTR, where no obvious Bragg peak due to A-oriented CaF_2 appears close to $L = 2/3$ (cf. Figure 4 and Table I), which could quite easily be resolved, since the Si(0,1,2/3) Bragg peak is forbidden, due to the diamond structure of Si (cf. the significant intensity of the analogous Bragg peak due to B-oriented CaF_2 on the (10) CTR for $L \simeq 2/3$). A more detailed CTR analysis yields an upper limit of 5% A-oriented CaF_2.

Furthermore, the L-dependence of these CTRs were completely analyzed using kinematic diffraction theory. Following Ref. 35, we modeled the CaF_2 films by two lateral separated CaF_2 phases (two columns). One column models the relaxed CaF_2, while the second column models the pseudomorphic part. The analysis shows that the relaxed CaF_2 phase assumes the bulk value for the vertical lattice constant (316 pm). Thus, this part of the CaF_2 film is completely relaxed and no residual strain can be detected. For the pseudomorphic part, however, the determined vertical lattice constant of 319 pm is slightly expanded, due to the tensile stress at the CaF_2/Si(111) interface.

2. Ge/CaF_2/Si(111)

Figure 7 shows in-plane scans in radial direction ($H = K$) of the (11L) CTR obtained from the Ge/CaF_2/Si(111) sample for small vertical scattering vectors L. Besides the extremely sharp Si peak at $K = 1.000$, there are two additional peaks, which are much broader than the Si peak. The in-plane scans were fitted to superimposed modified Lorentzians to obtain lateral lattice constants and grain sizes of the films. This analysis shows that the broad peak next to the Si peak is due to relaxed CaF_2, as reported above for the sample without Ge film. The position of the peak on the very left hand at $K = 0.959$ shows that it is caused by (laterally) relaxed Ge. From the halfwidths of both peaks, it can be estimated that both the CaF_2 and Ge grains have average lateral sizes of approximately 50 nm (agreeing well with the XRD analysis of the (00) rod presented above). In addition, we had to assume two more peaks under the Si peak to model also the wings on the right side of the Si Bragg peak. These peaks are situated on the Si peak position, but are

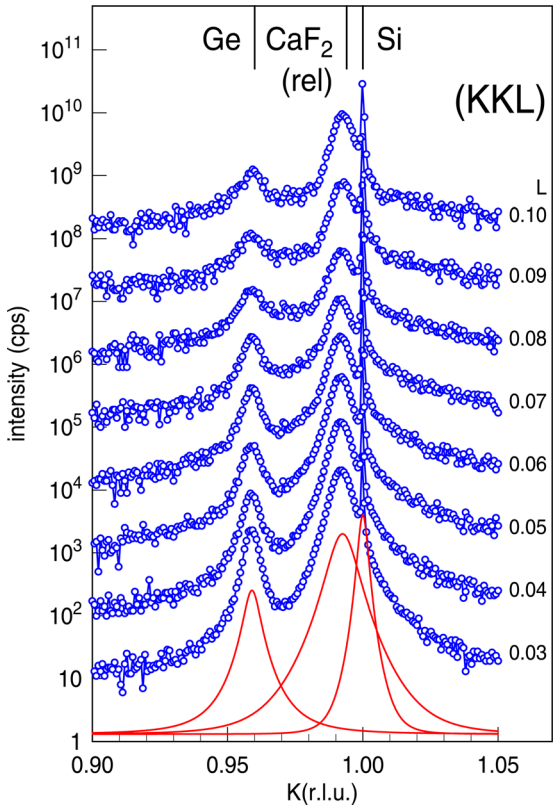

FIG. 7. (Color online) In-plane scans of the $(11L)$ CTR. The three immediately visible diffraction peaks are due to relaxed Ge film, the relaxed CaF_2 film, and the Si(111) substrate (from left to right). In addition, a peak due to pseudomorphic CaF_2 has to be assumed to describe the scans completely. Solid lines (shifted for clarity) show the contributions of the different films to the diffraction pattern at $L = 0.03$.

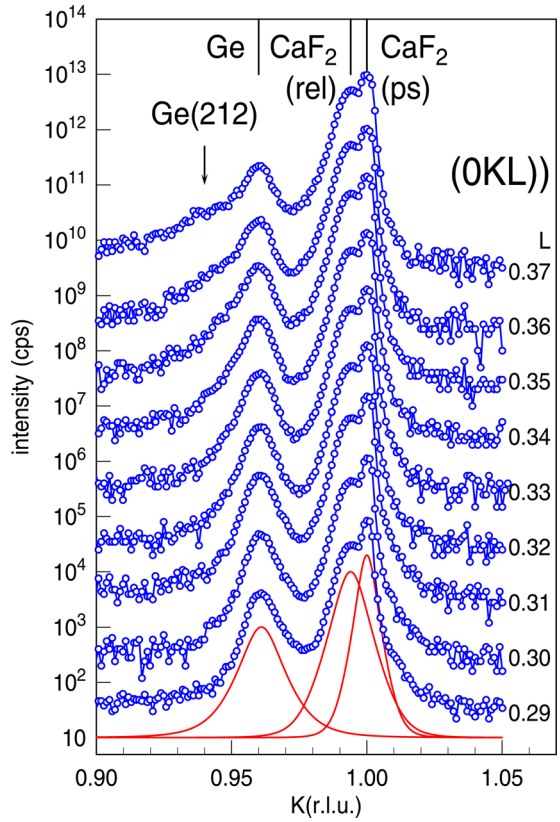

FIG. 8. (Color online) In-plane scans of the $(01L)$ CTR. The three peaks are due to relaxed Ge, relaxed CaF_2, and pseudomorphic CaF_2(from left to right). Solid lines represent fits of the different contributions to modified Lorentzians for $L = 0.29$.

broader than the Si peak and have lower intensity. Therefore, they can be assigned to the pseudomorphic phase of the CaF_2 film (grain size 120 nm) as well as diffuse scattering due to interface roughness (cf. results for CaF_2/Si(111) presented above).

Similar in-plane scans are additionally recorded for the $(10L)$ CTR and the $(01L)$ CTR to clarify the orientation of the Ge film. Figure 8 presents the in-plane scans for the $(01L)$ CTR for $L \simeq 1/3$ to be sensitive to B-oriented parts of the films. Please note that the orientation of the Ge film is presented in relation to the Si(111) substrate. On first sight, three peaks can obviously be distinguished, due to pseudomorphic CaF_2 ($K = 1.000$), relaxed CaF_2 ($K = 0.994$), and relaxed Ge ($K = 0.959$) (from right to left). As just reported for the $(11L)$ CTR, the peaks due to relaxed CaF_2 and Ge have similar FWHM, while the peak due to pseudomorphic CaF_2 is sharper, due to larger pseudomorphic CaF_2 grains. The latter peak can clearly be observed here because of the B-orientation of the CaF_2 film, since it is not curtained by the superimposed Si diffraction signal for this reason.

In addition to the three different peaks reported up to here, the $(01L)$ CTR shows an additional, but weak peak, which is labeled for the topmost curve by an arrow in Fig. 8. The position of this peak, however, shifts linearly if the vertical vector L is changed. Furthermore, its position matches the position of the bulk Bragg peak due to the relaxed Ge(111) film for $L = 0.32$ (vertical scattering vector of the Bragg peak of bulk Ge). Therefore, this peak is caused by facets of the Ge film. The analysis of the peak position with respect to the vertical scattering vector proves that the B-oriented Ge film has (212) facets. Corresponding results have also been obtained for Ge from the $(10L)$ CTR investigated for $L \simeq 1/3$. Especially, we observe diffraction peaks due to relaxed A-oriented Ge, which exhibits Ge(212) facets too.

Figure 9 presents the detailed analysis of the in-plane scans for both the $(10L)$ CTR and the $(01L)$ CTR. For the $(01L)$ CTR, the L dependences of both intensities due to pseudomorphic CaF_2 (open dots) and due to relaxed CaF_2 (open diamonds) show clearly fringes due to the homogeneous and identical thickness (12 TL) of both phases. Compared to this, the diffraction intensity from the B-oriented Ge exhibits no fringes, confirming that the film is very rough.

The complementary analysis of the $(10L)$ CTR demonstrates that the Si$(10L)$ CTR (open dots) exhibits strongly decreasing intensity due to the half infinite substrate, if the vertical diffraction scattering deviates from its value for the (bulk) Bragg peak ($L = 1/3$). Furthermore, we observe diffuse scattering on the Si rod (open diamonds) due to residual roughness at the CaF_2-Si interface, which may be superimposed by diffraction from small A-oriented fractions of the CaF_2 film mentioned above. The diffraction intensity of the A-oriented Ge does not show any fringes (equivalent to B-oriented Ge reported for the $(01L)$ CTR). Thus, the A-oriented parts of the Ge film are also very rough. Both the

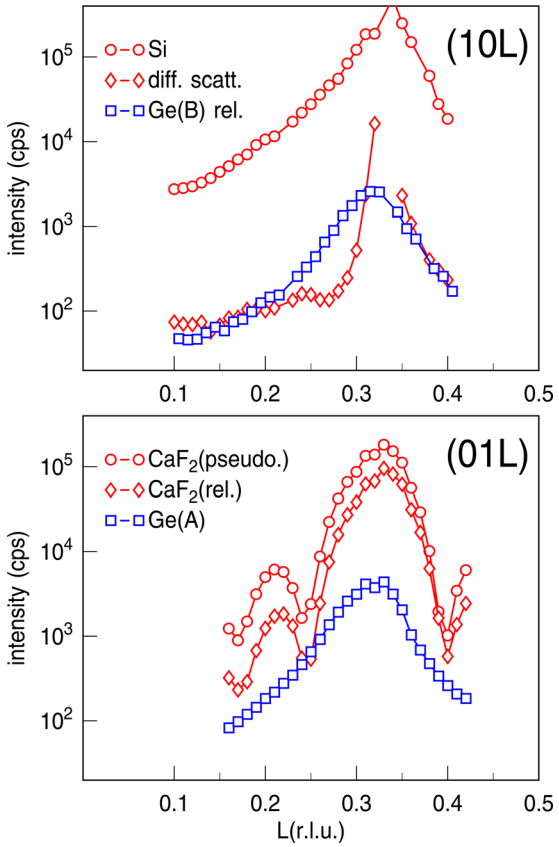

FIG. 9. (Color online) Analysis of the intensities of the different peaks of the in-plane scans of both $(10L)$ CTR and $(01L)$ CTR (cf. Fig. 8). The oscillations of the intensities of the peaks due to CaF_2 demonstrate the extreme homogeneity of the film thickness. The peaks due to Ge do not show oscillations, since the film thickness is inhomogeneous.

maximum intensity of the Ge CTR and its FWHM match the results obtained for the B-oriented Ge. Thus, there is no preference to one of these phases, neither for the amount of Ge nor for the average lateral grain size.

Furthermore, Ge Bragg peaks of both CTRs (due to A-oriented and B-oriented Ge) show an azimuthal broadening of $\pm 0.1^\circ$ compared to the azimuthal halfwidth of both Si(111) substrate and CaF_2 film. Thus, the relaxation of the Ge film is accompanied by some small azimuthal disorder (texture).

Finally, the L dependence of the CTRs has been investigated with lower lateral resolution (cf. above for the sample without Ge film) to determine the vertical crystalline structure of the films from the structure factor. Thus, the diffraction intensity from the CaF_2 film and the Si(111) substrate are recorded simultaneously (including interference effects between the substrate and pseudomorphic part of the CaF_2 film). Nevertheless, the Ge diffraction signal was well separated, due to the larger lateral mismatch of the relaxed Ge film. Therefore, the Ge CTRs are recorded separately. Just as for the first sample, the CTR intensities are recorded rotating the sample with respect to its surface normal to separate the CTR signal from the background.

The resulting structure factors are presented in Fig. 10. The results for the CaF_2/Si(111) CTRs (H, $K=1.00$) match the results of the sample without Ge. First, the CaF_2 films are B-oriented to an overwhelming majority. Second, the thickness of the CaF_2 is very homogeneous, as concluded from the very well-developed fringes. Thus, the Ge film does not influence the structure and morphology of the CaF_2 films.

Both Ge CTRs (H, $K=0.96$) show three Bragg peaks, as expected if the Ge film exhibits A-oriented *and* B-oriented parts (cf. Figure 4). The Ge Bragg peaks for $L=0.32$ are more symmetric than the Bragg peaks for higher values of L. This effect can be attributed to the higher lateral resolution of the experiment for small vertical scattering vectors L. Thus, for L close to 1/3, the Ge Bragg peaks are better separated from the Bragg peaks of Si and CaF_2, respectively, while the strong Si and CaF_2 Bragg peaks influence the measurement of the Ge Bragg peaks for higher values of L. The L positions of the Ge Bragg peaks match the positions calculated for bulk Ge. Thus, the Ge film is also completely relaxed in the vertical direction. The Ge Bragg peaks at $L=0.32$ were fitted to Lorentzians, since they are better resolved than the other Ge Bragg peaks. Taking the pure FWHM of these Bragg peaks, one would conclude an average Ge film thickness of 33 BL (10.7 nm). This result overestimates the Ge film thickness, since the rough Ge film

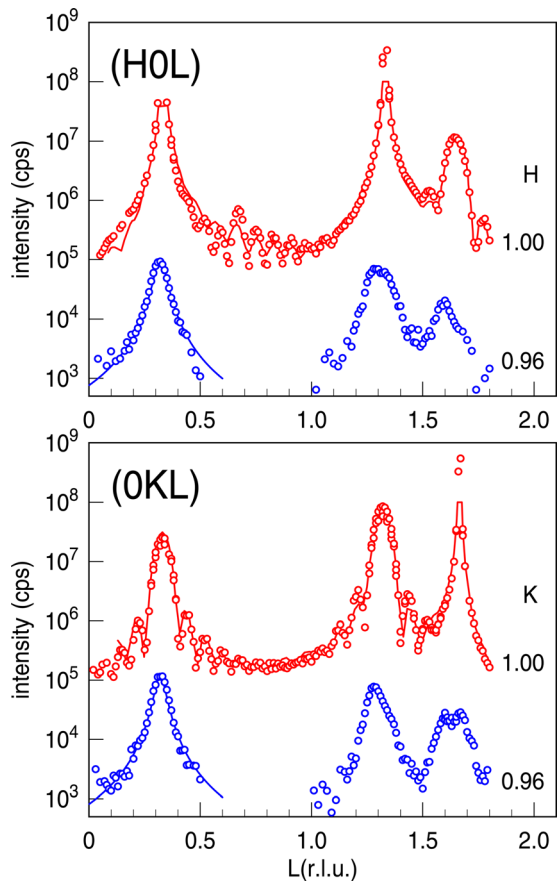

FIG. 10. (Color online) CTR analysis of the $(H0L)$ CTR (top) and $(0KL)$ CTR (bottom) for Ge/CaF_2/Si(111) for relaxed Ge (H, $K=0.96$) and the interfering CaF_2 and Si(111) (H, $K=1.00$). The CTRs for H, $K=1.00$ show that the CaF_2 film is B oriented and very homogeneous. The CTRs for H, $K=0.96$ demonstrate that the Ge film is relaxed and exhibits both A-oriented as well as B-oriented parts. Open dots show experimental results. The solid lines for H, $K=1.00$ are calculated from kinematic diffraction theory. The solid lines for the Ge CTRs for $L \simeq 0.32$ are fit to Lorentzians because of the rough and inhomogeneous Ge film.

surface leads to a more drastic decrease of the wings of the Bragg peak. Thus, the CTR results do not contradict the former XRR and XRD results.

IV. DISCUSSION AND CONCLUSION

Our synchrotron radiation–based experiments (XRR, XRD, GIXRD) on both CaF_2/Si(111) and Ge/CaF_2/Si(111) demonstrate that the crystalline structure of these layered structures can be characterized to a large extent.

For instance, we established with our studies that the 12TL CaF_2 film grown at 500 °C breaks up into two phases: one pseudomorphic phase and one relaxed phase. This effect has recently been demonstrated for thinner CaF_2 films (thickness < 7 TL, mainly deposited at 600 °C) and attributed to the formation of partial edge dislocations at substrate steps.[35] Before, the formation of dislocation lines and the correlation were reported from plan-view TEM studies.[36]

Compared to these former studies, on one hand, the amount of relaxed CaF_2 is larger here, due to the increased film thickness driving the system to a higher degree of relaxation. On the other hand, the vertical lattice constants of both phases agree with the previously reported vertical lattice constants. Complete relaxation (determined from the vertical CaF_2 lattice constant of 315.5 pm) has also been reported for 15TL CaF_2 deposited on Si(111) at 720 °C by Lucas *et al.*,[36] while they obtained a vertical lattice constant of 317.4 pm for a 10-nm film grown by a template procedure with initial growth at 700 °C.[37] Applying a similar two step template growth technique (first deposition of 2 nm CaF_2 at 750 °C followed by deposition of additional 10 nm at 10 °C), the latter vertical lattice constant was also reported by other authors.[38,39] Thus, in these cases, the reported lattice constants, which have an intermediate value compared to the lattice constants reported here, may be due to an averaged vertical lattice constant of pseudomorphic parts and relaxed parts of the CaF_2 film. The lateral CaF_2 grain size of 60 nm determined from in-plane scans for the relaxed phase coincides very well with the value of 54 nm expected from the lattice mismatch. Thus, the lateral grain size of the relaxed phase seems to be confined by the formation of (interface) dislocations.

Compared to the very homogeneous CaF_2 (cf. well-developed fringes of all CTRs), the Ge film is very rough, as proven by our XRR analysis and the missing fringes of the GIXRD investigations. The large roughness of the Ge film is also observed in supplemental studies with atomic force microscopy (AFM), which show the formation of large islands (island diameter approximately 80 nm) and rms-roughness of several nanometers. The inhomogeneity of the Ge film thickness can also be judged from x-ray photoelectron spectroscopy (XPS), where more Ca2p and F1s photoelectrons are detected than expected for a homogeneous Ge film of 8.4 nm thickness. Furthermore, we observe a slight increase of the ratio between Ca2p and F1s photoelectrons, which can be attributed to (partial) segregation of Ca to the surface at the Ge film. This has to be compared with the growth of 200-nm-thick Ge films on CaF_2 films with predeposited boron, where Ca segregation is suppressed, as demonstrated by SIMS studies.[16]

While homogeneous Ge films are formed via deposition at room temperature,[28] annealing studies by electron spectroscopy show that ultrathin Ge films are gradually rearranged via formation of Ge islands.[28,29] The rearrangement starts at 200 °C for ultrathin Ge films of less than 2 nm thickness and, finally, leads to Ge islands of 11–12 BL (≈4 nm) height after annealing at 600 °C.[28,29] Thus, it can be expected that the roughening and de-wetting behavior due to annealing is less drastic for the thicker Ge film studied here (thickness 8.4 nm), which is also annealed at 600 °C. In addition, one expects improvement and less rough Ge films in our case, since the film is additionally exposed to the surfactant Sb, which reduces the surface energy of Ge. Indeed, we observe that the Ge film does not entirely de-wet and does not form 3D Ge islands, although the surface of the Ge film is a very rough surface, as concluded from all experiments. Furthermore, we conclude from XPS that Sb is only very little incorporated into the Ge film, in agreement with results reported for the Sb surfactant-mediated epitaxy of Ge on Si(111).[25]

Complete relaxation has been reported for 200-nm-thick Ge films on CaF_2/Si(111).[16] Our synchrotron radiation–based XRD and GIXRD experiments show that ultrathin Ge films of 8 nm thickness are already completely relaxed (both in vertical and lateral direction) after annealing at 600 °C. Furthermore, we observe the formation of A-oriented and B-oriented phases with equal parts. The formation of A/B-twins due to stacking faults has been reported before for thin CaF_2 films (thickness 250 nm, growth temperature 600 °C).[14] The authors proposed that the twinning starts from the formation of both A-oriented and B-oriented Ge islands during the early nucleation stages. Compared to this, Ge(111) films are preferentially B orientated (with respect to the CaF_2 film) when boron has been deposited before Ge deposition.[16] Therefore, the structure of the Ge-CaF_2 interface plays an important role for the orientation of the Ge(111) films, as pointed out recently from DFT calculations.[12] Furthermore, the latter authors report that the amount of B-orientated Ge(111) increases if the deposition temperature is increased. This effect is similar to the well-known structure of the CaF_2-Si(111) interface, where CaF_2 is reduced to CaF at higher deposition temperatures, inducing the growth of B-oriented CaF_2(111) films.[7] Therefore, B-oriented Ge(111) films can be related to the Ge-Ca-F interface.

Our studies, however, show equal parts of A-oriented and B-oriented Ge phases. Therefore, we assume that fluorine is only partly removed from the CaF_2 interface due to Ge deposition at room temperature, although room temperature–deposited Ge films are single crystalline.[28] Therefore, it is reasonable that both A-oriented and B-oriented islands are initially formed during room temperature deposition, while twin boundaries are subsequently formed when the islands coalesce. Obviously, post deposition annealing cannot remove these twin boundaries. Furthermore, we like to mention that Si films prepared on CaF_2 via SE-SPE (using B or Sb) also show the formation of stacking twin due to A-oriented and B-oriented parts of the films.

Thus, one can speculate whether fluorine removal (e.g., by electron bombardment) leads to the formation of Ge films

without twin boundaries, as previously reported for ultrathin Si deposited on CaF_2 films, which are modified first by electron bombardment and then by As deposition.[18] The stronger binding of room temperature–deposited Ge films to CaF_2 films exposed to electron bombardment has also been concluded before from XPS studies.[29]

It is remarkable that the average lateral size of the Ge grains matches the average lateral size of the *relaxed* CaF_2 grains. Probably, Ge nucleates preferentially on relaxed CaF_2, since both the lateral and the vertical lattice constants of relaxed CaF_2 are closer to the Ge bulk lattice constant. Another explanation may be that the increase of Ge grain size is confined by the grain boundaries of the CaF_2 film.

The Ge film does not show only randomly distributed surface roughness, but forms {221} facets during annealing. This is surprising, since, in contrast to this, the formation of {113} facets and {331} facets is often observed for Ge/Si(111). We like to mention, however, that the formation of {221} facets is also reported for Ge epitaxy on Si(331).[40]

Finally, the success of Sb as surfactant for solid phase epitaxy of $Ge/CaF_2/Si(111)$ has to be compared to the effectiveness of surfactants during SE-SPE of $Si/CaF_2/Si(111)$. Using Sb or B as surfactant, it was demonstrated for 11-nm-thick Si films, which were deposited at room temperature on $CaF_2/Si(111)$ and subsequently annealed to 635 °C, that the Ge films were very smooth with rms-roughness of less than 1 nm.[20,21] Compared to these results, the Ge film is much rougher (rms-roughness 4.1 nm), although the tendency to form 3D islands should be less pronounced for Ge compared to Si, since the Ge surface energy is smaller than the Si surface energy. Furthermore, the Ge surface energy is additionally decreased by the adsorbed Sb. Thus, the increased roughness can be attributed to both a higher mobility of Ge compared to Si and to a weaker binding of Ge at the interface. Therefore, these results demonstrate the importance to tailor also the Ge-CaF_2 interface energy. Besides the use of surfactants, one probably has to add interfactants to increase the interface binding and to force the wetting of CaF_2 by Ge. One possibility may be to pre-deposit B, as demonstrated by Cho *et al.*[16] for a Ge film of several 100 nm thickness. Another possibility is to use a more gentle annealing, which may sufficiently re-crystallize Ge films without breaking into islands. These studies are under investigation.

In conclusion, we characterized $CaF_2/Si(111)$ and $Ge/CaF_2/Si(111)$ with synchrotron-based radiation. The latter structure has been fabricated with surfactant (Sb)-enhanced SPE. On the one hand, the CaF_2 film is very smooth, with homogeneous thickness, although the formation of two phases (relaxed and pseudomorphic) was verified. On the other hand, the Ge film is completely relaxed, but very rough. Therefore, Sb does not completely suppress the dewetting tendency of Ge films at 600 °C, as observed for SE-SPE of $Si/CaF_2/Si(111)$. We attribute this effect to the higher mobility of Ge compared to Si.

ACKNOWLEDGMENTS

We kindly acknowledge financial support by the Deutsche Forschungsgemeinschaft (DFG) projects Wo 633/6-1 and Ho1885/3-1. Furthermore, S. Bessedine and O. Seeck are acknowledged for support at beamlines BW2 and W1, respectively, for synchrotron experiments carried out at HASYLAB/DESY. DESY is a member of the Helmholtz Association (HGF).

[1] J. D. Cressler, *Silicon Heterostructures Handbook* (CRC, Taylor & Francis, London, 2006).
[2] T. Akatsu, C. Deguet, L. Sanchez, F. Allibert, D. Rouchon, T. Signamarcheix, C. Richtarch, A. Boussagol, V. Loup, F. Mazen, J.-M. Hartmann, Y. Campidelli, L. Clavelier, F. Letertre, N. Kernevez, and C. Mazure, Mater. Sci. Semicond. Process. **9**, 444 (2006).
[3] C. Claeys and E. Simoen, *Germanium-Based Technologies: From Materials to Devices* (Elsevier, New York, 2007).
[4] F. Dimroth and S. Kurtz, MRS Bull. **32**, 230 (2007).
[5] R. R. King, D. C. Law, K. M. Edmondson, C. M. Fetzer, G. S. Kinsey, H. Yoon, R. A. Sherif, and N. H. Karam, Appl. Phys. Lett. **90**, 183516 (2007).
[6] L. J. Schowalter and R. W. Fathauer, Crit. Rev. Solid State Mater. Sci. **15**, 367 (1989).
[7] M. A. Olmstead, in: *Thin Films: Heteroepitaxial Systems*, edited by W. K. Liu and M. B. Santos (World Scientific, Singapore, 1999), p. 211.
[8] J. Wollschläger, in: *Recent Research Developments in Applied Physics*, edited by S. G. Pandalai, (Transworld Research Network, Trivandrum, 2002), Vol. 5–11, p. 621.
[9] J. Wollschläger, Appl. Phys. A **75**, 155 (2002).
[10] T. Asano and H. Ishiwara, Jpn. J. Appl. Phys. **21**, L630 (1982).
[11] L. J. Schowalter and R.W. Fathauer, J. Vac. Sci. Technol. A **4**, 1026 (1986).
[12] T.-L. Chan, C. Gaire, T.-M. Lu, G.-C. Wang, and S. B. Zhang, Surf. Sci. **604**, 1645 (2010).
[13] S. Kanemaru, H. Ishiwara, T. Asano, and S. Furukawa, Surf. Sci. **174**, 666 (1986).
[14] R. W. Fathauer, N. Lewis, E. L. Hall, and L. J. Schowalter, J. Appl. Phys. **60**, 3886 (1986).
[15] S. Kanemaru, H. Ishiwara, and S. Furukawa, J. Appl. Phys. **63**, 1060 (1988).
[16] C. C. Cho, H. Y. Liu, L. K. Magel, and J. M. Anthony, Appl. Phys. Lett. **63**, 3291 (1993).
[17] M. Watanabe, Y. Iketani, and M. Asada, Jpn. J. Appl. Phys. **39**, L964 (2000).
[18] C. R. Wang, B. H. Müller, E. Bugiel, and K. R. Hofmann, Appl. Surf. Sci. **211**, 203 (2003).
[19] C. R. Wang, B. H. Müller, E. Bugiel, T. Wietler, M. Bierkandt, K. R. Hofmann, and P. Zaumseil, J. Vac. Sci. Technol. A **22**, 2246 (2004).
[20] J. Wollschläger, C. Deiter, M. Bierkandt, A. Gerdes, M. Bäumer, C. R. Wang, B. H. Müller, K. R. Hofmann, and P. Zaumseil, Surf. Sci. **600**, 3637 (2006).
[21] C. R. Wang, B. H. Müller, E. Bugiel, and K. R. Hofmann, IEEE Trans. Nanotechnol. **2**, 236 (2003).
[22] C. R. Wang, B. H. Müller, and K. R. Hofmann, Nanotechnology **14**, 1192 (2003).
[23] C. R. Wang, M. Bierkandt, S. Paprotta, T. Wietler, and K. R. Hofmann, Appl. Phys. Lett. **86**, 033111 (2005).
[24] B. R. Schroeder, S. Meng, A. Bostwick, and M. A. Olmstead, Appl. Phys. Lett. **77**, 1289 (2000).
[25] M. Horn-von Hoegen, M. Copel, J. C. Tsang, M. C. Reuter, and R. M. Tromp, Phys. Rev. B **50**, 10811 (1994).
[26] P. W. Deelman, T. Thundat, and L. J. Schowalter, Mater. Res. Soc. Symp. Proc. **358** 139 (1995).
[27] A. I. Yakimov, A. S. Derjabin, L. V. Sokolov, O. P. Pchelyakov, A. V. Dvurechenskii, M. M. Moiseeva, and N. S. Sokolov, Appl. Phys. Lett. **81**, 499 (2002).
[28] E. P. Rugeramigabo, C. Deiter, and J. Wollschläger, Appl. Surf. Sci. **254**, 143 (2007).
[29] M. A. Olmstead and R. D. Bringans, Phys. Rev. B **41**, 8420 (1990).
[30] C. R. Wang, B. H. Müller, and K. R. Hofmann, Thin Solid Films **410**, 72 (2002).
[31] E. Vlieg (University of Nijmegen, The Netherlands). The ANA-ROD project has the internet address: http://www.esrf.eu/computing/scientific/joint_projects/ANA-ROD/.

[32]F. Bertram B.Sc. thesis (Universität Osnabrück, 2007).
[33]L. G. Parratt, Phys. Rev. **95**, 359 (1954).
[34]L. Nevot and P. Croce, Rev. Phys. Appl. **15**, 761 (1980).
[35]C. Deiter, M. Bierkandt, A. Klust, C. Kumpf, Y. Su, O. Bunk, R. Feidenhansl, and J. Wollschläger, Phys. Rev. B **82**, 085449 (2010).
[36]C. A. Lucas and D. Loretto, Appl. Phys. Lett. **60**, 2071 (1992).
[37]C. A. Lucas, D. Loretto, and G. C. L. Wong, Phys. Rev. B **50**, 14340 (1994).
[38]J. Harada, I. Takahashi, Y. Itoh, N. S. Sokolov, N. L. Yakovlev, Y. Shusterman, and J. C. Alvarez, J. Cryst. Growth **163**, 31 (1996).
[39]Y. Itoh, I. Takahashi, A. Ichimiya, J. Harada, and N. S. Sokolov, J. Cryst. Growth **166**, 61 (1996).
[40]H. Omi and T. Ogino, Phys. Rev. B **59**, 7521 (1999).